Final Draft

of the original manuscript

Snihirova, D.; Wang, L.; Lamaka, S.; Wang, C.; Deng, M.;
Vaghefinazari, B.; Höche, D.; Zheludkevich, M.:

Synergistic Mixture of Electrolyte Additives: A Route to a High-Efficiency Mg–Air Battery.

In: The Journal of Physical Chemistry Letters. Vol. 11 (2020) 20, 8790 - 8798.
First published online by ACS: 28.09.2020

https://dx.doi.org/10.1021/acs.jpclett.0c02174

Synergistic mixture of electrolyte additives: a way to high efficiency Mg-air battery

Darya Snihirova[*1], Linqian Wang[1], Sviatlana V. Lamaka[1], Cheng Wang[1], Min Deng[1], Bahram Vaghefinazari[1], Daniel Höche[1], Mikhail L. Zheludkevich[1, 2].*

1 MagIC—Magnesium Innovation Center, Helmholtz-Zentrum Geesthacht (HZG), 21502 Geesthacht, Germany

2 Institute of Materials Science, Faculty of Engineering, Kiel University, 24143 Kiel, Germany

ABSTRACT Magnesium primary cells are currently experiencing a renaissance following the suggestions of new strategies to boost their performance. The strategies suggested will still maintain utilization efficiencies of 30-70%, which is considered to be relatively modest. In this work a highest ever reported level of utilization efficiency of 82% is achieved for a Mg-based primary cell using a synergistic combination of electrolyte additives. It is demonstrated that a joint use of sodium nitrate and salicylate as electrolyte additives allows to reach the aforementioned utilization efficiency at 5 mA/cm2 via offering an effective suppression of anode self-corrosion and uniform Mg dissolution under discharge conditions.

KEYWORDS magnesium anode, suppression of self-corrosion, nitrate, salicylate, discharge, aqueous electrolyte, utilization efficiency

TOC GRAPHICS

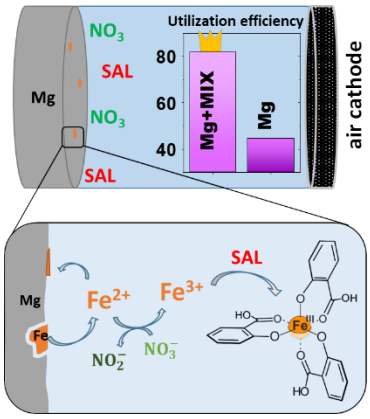

Lately, Mg-air batteries have gained tremendous popularization and are an active topic of research. The merits of Mg-air systems, when compared to the usual Li batteries, are seen to have no safety limitation, reduced costs, and have high gravimetric energy density. Primary Mg-air batteries attributed to the excellent theoretical electrochemical properties of Mg metal, like the high theoretical energy density and relatively negative electrode potential (− 2.37 V versus − 3.05 V of Li (vs. SHE)). Moreover, Mg-air batteries also have the advantage of low cost of corresponding anode metal (≈$1 per kWh) compared with Li-ion batteries (≈$200-300 per kWh) or Li-air batteries (≈$50 per kWh), high safety, and environmental benignity[1]. They are non-toxic, robust primary batteries of straightforward operation, exhibiting a significant advantage regarding energy density to cost [2]. Though there is a noticeable recent evolution of primary Mg-air batteries [3-4], they continue to face obstacles, related to reactivity of Mg in aqueous electrolyte. In practice, unwanted self-corrosion reduces anode utilization efficiency during discharge of Mg-air battery (*eq. S1*).

To date, the approach to improve the anode performance was mainly focused on the alloy development. Through the optimization of the composition of the alloy, there will be an improvement in the discharge potential and reduction in the self-corrosion rate. According to

literature, the utilization efficiency may reach 60% at current density of 5 mA/cm^2 for Mg-Al-Ga [5] or Mg-Ca [6] alloys, which is considered to be high for Mg-air batteries with aqueous electrolytes (Figure 1a). The increase in utilization efficiency, especially at higher discharge current densities, was attributed to improved corrosion resistance via addition of Ga, Sn or In to Mg-Al [5, 7-8]. Besides these alloy, there has been a depiction of the significant improvement in voltage and specific energy of the battery through the alloying of Mg with a small amount of Ca. [6]. A more comprehensive overview on the alloy development for Mg-air batteries could be found elsewhere [3-4, 9]. An important motivation for this work to further increase the utilization efficiency of Mg-air battery was the straightforward approach to influence the electrochemical reaction on the anode via electrolyte modifications. In the last four years, attempts to use corrosion inhibitors as electrolyte additives were explored. Several anions such as vanadates [10], phosphates [10-12], nitrates [11], chromates [13] or organic molecules [14-16] were investigated. Often the improvement of the discharge capacity was low or even negative effects occurred. The adequate efficiency was not reached yet, probably because most of the corrosion inhibitors for Mg passivate the surface by forming insoluble precipitates or adsorbed layers. Indeed, they are not suitable for Mg-air batteries when a blocking layer on the anode is formed. A clear and more effective approach to decrease Mg corrosion without formation of the passivation layer during discharge was suggested recently [14]. During the dissolution of Mg, which contains high amount of noble impurities (iron content 178 ppm for commercially pure Mg used in this work, Table S1), micro-galvanic corrosion followed by detachment of iron particles occurs with their further dissolution producing Fe^{2+} ions and possibly further oxidation to Fe^{3+}. The formed cations might undergo direct reduction to metallic Fe, when in contact with highly electronegative Mg surface, as shown recently [17-18].

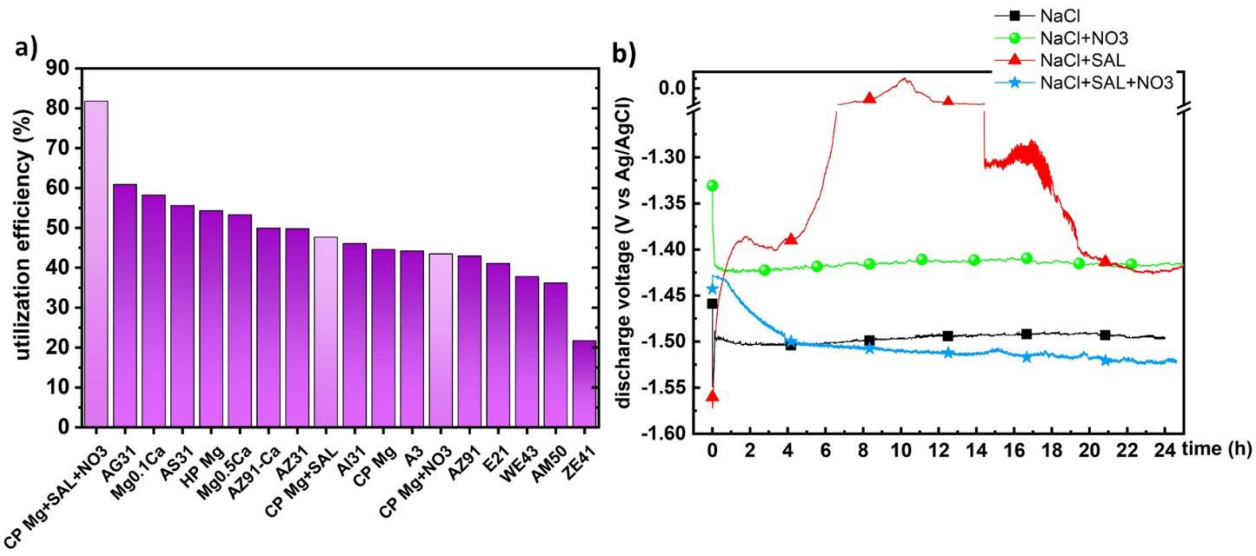

Figure 1 a) Comparison of the alloy performance (data were measured at comparable conditions 3.5% NaCl electrolyte, 5 mA/cm^2 discharge current density) [4-5, 9, 19].Details for alloy composition are given in Table S1. The utilization efficiency for CP-Mg with additives is identified as paled colour columns. b) Discharge curves for CP-Mg with (sodium nitrate (NO3), sodium salicylate (SAL) or their mixture) and without electrolyte additives in 3.5% NaCl at 5 mA/cm^2.

The re-deposited iron plays the role of the local cathode, promoting self-corrosion and leading to loss of utilization efficiency. The effective strategy for suppression of Mg corrosion was achieved by using Fe complexing agents [20-21] with their successful application for Mg-air batteries [14, 22-23]. It was shown that the additives that form soluble complexes with Fe influenced the Fe/Fe^{2+}/Fe^{3+} redox cycle and remarkably decreased self-corrosion of Mg during discharge. This discovery greatly widens the number of potential systems that may boost the performance of Mg-air battery. The first trials of using complexing agents as electrolyte additives showed that utilization efficiency of battery with micro-alloyed Mg-Ca anode was improved from 60% to 65% [23]. However, the search for the most efficient additives is still in its commencement. In this work, we propose to use a mixture of different additives in order to explore the synergistic effect. The

synergistic combination cannot be predicted a priori. As a consequence, the identification of the suitable additive combinations must be first based on experimentation. For aqueous Mg-air battery, the attempt to use the combination of sodium silicate and alginate, or sodium phosphate and dodecylbenzenesulfonate as electrolyte additives was reported [12, 24], however little or no improvements were observed in comparison with single additives. Apart from this, to the best of our knowledge, the mixtures of additives for aqueous Mg-air battery electrolytes have not been explored before. This paper gives an insight into the value obtained after employing a mixture of electrolyte additives: sodium nitrate and salicylate. Both anions, nitrate and salicylate, strongly influenced the oxidation and re-deposition cycle of Fe and, as a result, increased the anode efficiency in comparison with conventional aqueous electrolyte.

Figure 1(a) represents the anodic utilization efficiency at 5 mA/cm^2 discharge current in electrolyte containing 3.5% NaCl. A great escalation was noted in the value of utilization efficiency, which reached 82%. It is considerably higher than the previously reported values, which are usually below 60% for the same conditions. Comparison of specific energy or discharge potential from different studies calculated under different conditions (electrolyte concentration, discharge current density, different cathode materials) typically is not conclusive. For this reason, the utilization efficiency was chosen as an indicative parameter for accurate evaluation of the performance of the Mg battery.

The discharge curves of Mg anode in the electrolytes with selected additives and their mixtures are shown in Figure 1(b). The electrochemical tests were done using three electrodes cell with commercial purity Mg (CP-Mg) as working electrode, Ag/AgCl as a reference electrode and Pt wire as a counter electrode. (The experimental details are provided in the Supporting materials). The potential of the cell in salicylate (SAL) containing electrolyte was shifted towards positive

values after 4 h of discharge with further jump in potential after appx. 20 h of discharge. The presence of nitrate augmented the average potential to -1.41 V as compared to bare NaCl -1.50 V. The average cell potential of the half-cell with additive mixture was -1.50 V, which was similar to the discharge potential in reference NaCl electrolyte (Table 1). The main focus of this work was the self-discharge and self-corrosion of Mg anode, which always an issue that decreases the battery service life and energy density. Focusing on half-cell performance of one of the battery components, namely Mg anode, we would like to avoid limitations caused by cathodes, which may also contribute to the voltage drop. The results for full cell discharge are shown on Figure S1. The hydrogen evolved during discharge was collected by a set-up described elsewhere [9]. The inverted burette was placed over the embedded Mg sample for H_2 collection during 8h of half-cell discharge in order to calculate the H_2 evolution rate (HER).

Table 1 Comparison of CP-Mg properties in different electrolytes under discharge current density 5 mA/cm^2. *Calculations are based on hydrogen evolution rate during discharge.

Electrolyte	**Average discharge potential (V vs Ag/AgCl)**	**H_2 evolution during discharge (µmol cm^{-2} min^{-1})**	**Inhibition efficiency of HER* (%)**	**NO_2^- evolution during discharge (µmol cm^{-2} min^{-1})**
3.5% NaCl	-1.52±0.05	1.89±0.62		
3.5% NaCl+NO_3^-	-1.42±0.01	1.00±0.21	47	0.08±0.002
3.5% NaCl+SAL	-1.16±0.05	1.64±0.29	13	
3.5% NaCl+MIX	-1.50±0.02	0.43±0.19	77	0.02±0.005

The inhibition efficiency of HER was calculated by following equation

$$IE\ (\%) = \frac{HE_{uninhibited} - HE_{inhibited}}{HE_{uninhibited}} \times 100\%$$

Where $HE_{uninhibited}$ is the hydrogen evolution rate without additives, $HE_{inhibited}$ is hydrogen evolution rate in presence of electrolyte additives. The quantification of NO_2^- was done based on Griess method (DIN EN 26777). Briefly, the aliquots of electrolyte were collected during discharge, with following dilution mixed with Lunges reagent and brought for spectrophotometric analyses (more details are given in Supporting Information). All the measurements were done twice to ensure the reproducibility.

The surface of the anode after discharge was inspected by Scanning Electron Microscopy (SEM). The micrographs of Mg anode cross-section are shown in Figure 2. The corrosion products were found on the surface after discharge in NaCl (Figure 2 (a, b)), SAL (Figure 2 (c, d)) and NO_3^- (Figure 2 (e, f)) electrolytes. Notably, the presence of SAL leads to the formation of a thicker layer of precipitates that blocks the anode surface and battery fails due to high IR drop through the deposited layer.

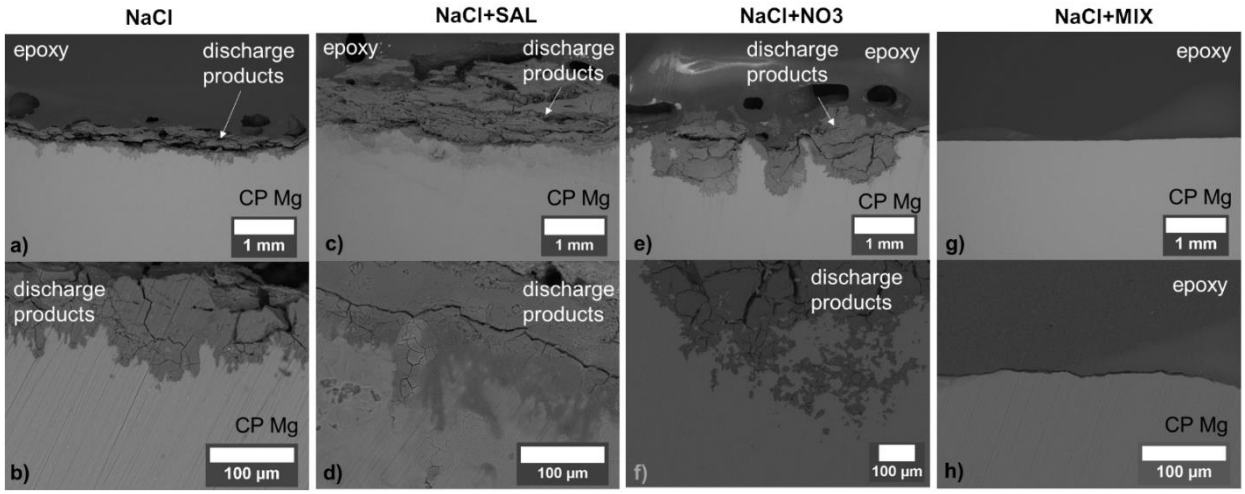

Figure 2. Micrographs of CP-Mg samples after 24h discharge at 5 mA/cm2 current density (cross-section). (a, b) after discharge in 3.5% NaCl, (c, d) 3.5%NaCl+SAL, (e, f) 3.5%NaCl+NO_3, (g, h) 3.5%NaCl+MIX.

The surface conditions of magnesium anode before and after the discharge were accessed by electrochemical impedance spectroscopy (EIS) (Figure 3). The impedance of CP-Mg in NaCl and NaCl+NO3 decreases after 24h of discharge, indicating lower protection of the surface film and thus lower IR drop through the discharge products. The addition of SAL shows lower impedance due to the ability to form soluble complexes with Mg^{2+} which activate the dissolution kinetic of the native oxide film [23]. However, after discharge, the increased values of impedance became evident for SAL. The rise of electrolyte resistance was possibly due to the growth of the the thicker and more compact layer of corrosion products by formation of smaller crystals of $Mg(OH)_2$ in the presence of SAL. Maltseva et al. [25] studied surface film evolution during Mg corrosion and reported that smaller flakes of magnesium hydroxide form in presence of SAL. Thus, growth of the protective layer may be the reason of fluctuation towards more positive values of discharge potential for NaCl+SAL.

Although salicylate was previously reported as a promising additive for Mg-air battery [14, 22-23], its performance becomes worse at higher discharge loads and in a more concentrated NaCl electrolyte. This can be attributed to the relatively less abundance of SAL to complex with swiftly generated Fe^{3+} and Mg^{2+} at the mentioned condition. Interestingly, the nitrate ion was reported as an efficient corrosion inhibitor [21, 26] and favorable electrolyte for Mg-air batteries [11, 15].

Clearly, in this work, when the harsher environment is used, nitrate reduced the utilization efficiency of Mg anode at the applied discharge current density of 5 mA/cm^2 and caused non-uniform dissolution with visible layer of corrosion products accumulated over the surface (Figure 2 (e, f)).

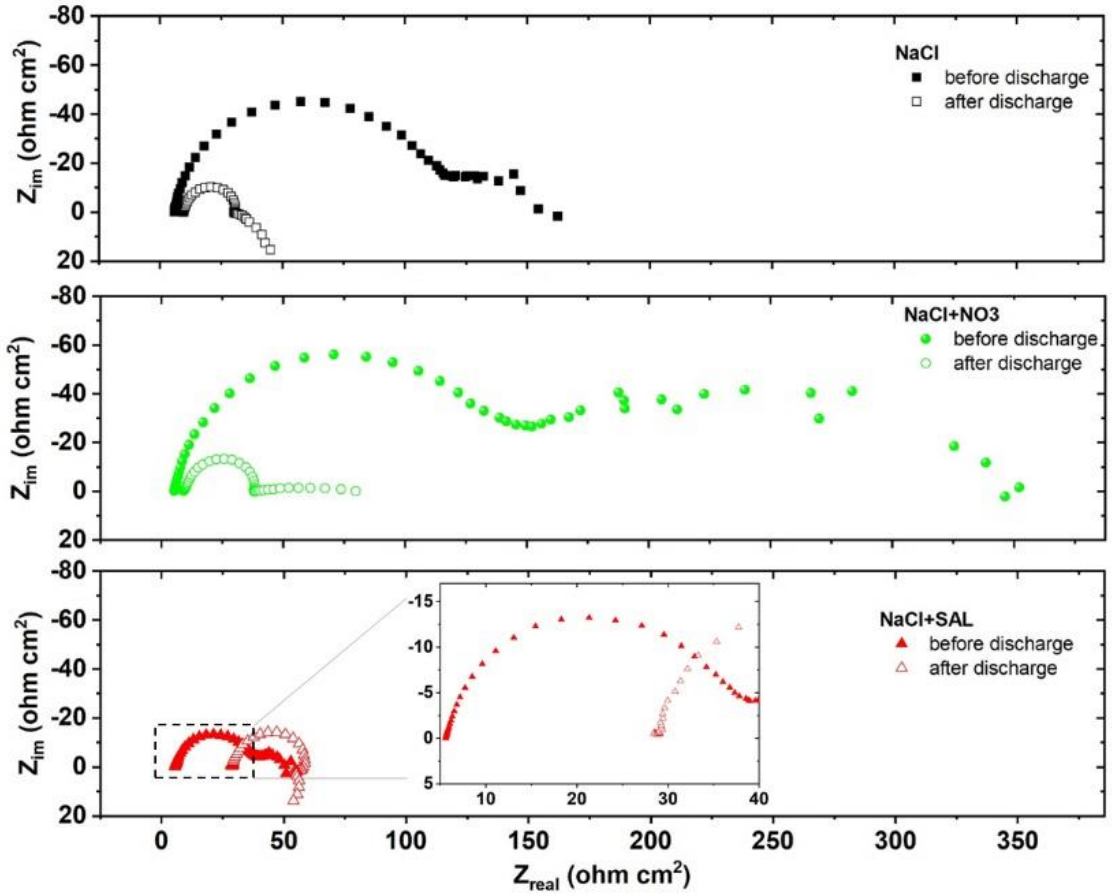

Figure 3 Comparison of the EIS for CP-Mg anode in different electrolytes (NaCl, NaCl+NO3 and NaCl+SAL) measured before and after 24h of discharge.

One reason for the diminution of efficiency is attributed to the chunk effect, namely unwanted spalling of metallic chunks from Mg anode during discharge. It can be seen from Figure 2 (f) that large Mg chunks are trapped by the corrosion products. The chunk effect decreases the anode utilization efficiency, especially at lower current densities [9]. One infers the rough surface generated as a result of the chunk effect solely; but it is not so, the presence of the NO_3^- itself may change the surface condition of Mg. The formation of a thin protective film on magnesium in nitrate-containing solution was shown by Richey et al. [11]. The film resistance was estimated by EIS and rated as high for NO_3^- in comparison with NaCl electrolyte. The higher impedance for NaCl+NO3

in comparison with NaCl was found also in this work (Figure 3) confirming the formation of protective film on the surface of CP-Mg with addition of NO_3^- to NaCl. However, to maintain an optimum potential during discharge, there should be a compromise between surface passivation and dissolution of Mg through the passive layer. At higher current density, the passive film may impede the fast Mg dissolution leading to non-uniform surface dissolution and relatively high charge transfer resistance of the Mg electrode.

Remarkable increase in utilization efficiency by mixture of additives is associated with the suppression of parasitic cathodic reactions on the anode and elimination of the chunk effect [9]. We assume that all the self-corrosion on the anode is accompanied by 3 processes: nitrate reduction (eq. 1), hydrogen evolution (eq. 2) and oxygen reduction (eq. 3). Here we analyze the contribution of electrolyte additives on each process. The hydrogen evolution measurements usually conclude on the effect of the self-corrosion on Mg anode efficiency [9]. However, O_2 reduction was reported as another cathodic process during Mg corrosion (eq. 3) [27-28]. Meanwhile, alkalization of the solution during corrosion of Mg, associated with cathodic processes (eq. 1, 2 and 3), was also recorded. Information about local pH will contribute to the clarification of the mechanism of the respective additives.

$$NO_3^- + H_2O + 2e^- \rightarrow NO_2^- + 2OH^- \quad (1)$$

$$2H_2O + 2e^- \rightarrow H_2 \uparrow + 2OH^- \quad (2)$$

$$O_2 + 2H_2O + 4e^- \rightarrow 4OH^- \quad (3)$$

Nitrate can play the role of an additional cathodic depolarizer [11] since it can be reduced to nitrite (eq. 1) at the potentials under the Mg discharge conditions. The reduction of nitrates on Mg may

also be a reason for the shift towards more positive electrode potential during the discharge (Figure 1b). Moreover, an additional cathodic process occurring during the discharge on the anode should cause a reduction of the Faradaic efficiency. Therefore, the kinetics of nitrite generation at the cathode as well as the rate of hydrogen evolution resulted from simultaneous water reduction (eq. 2) at the anode were measured.

The ***evolved H_2*** and NO_2^- concentration profiles are shown in Figure 4. The rate of parasitic reduction reaction was greatly influenced by additives, with the lowest volume of hydrogen evolved for Mg with the additive mixture. The reduction of nitrates to nitrites (eq. 1) also took place, however at a slower rate than the water reduction reaction. Based on the results, the contribution of NO_3^- reduction to the unwanted self-corrosion is estimated as 3.0% for NaCl+NO3 and 1.7% for NaCl+MIX in respect to the total parasitic cathodic reactions. Table 1 presents the results on the kinetics of both parasitic cathodic reactions. The mixture of additives effectively reduces H_2 evolution rate and also suppresses the NO_2^- formation. It is also clear that the main cathodic reaction on CP-Mg anode during discharge is water reduction. The inhibition efficiency of additives for CP-Mg was calculated based on hydrogen evolution rate and was equal to 77% for mixture SAL+NO3 (Table 1). The local gradient of ***dissolved oxygen*** over the corroding Mg surface was measured by fiber-optic micro optode (O_2 probe) simultaneously with pH monitoring in order to accurately investigate the influence of additives on Mg self-corrosion. The simultaneous measurements of local pH and concentration of dissolved oxygen were successfully demonstrated in the field of corrosion science [29-32]. In this study, the measurements of O_2 and pH were assessed during discharge.

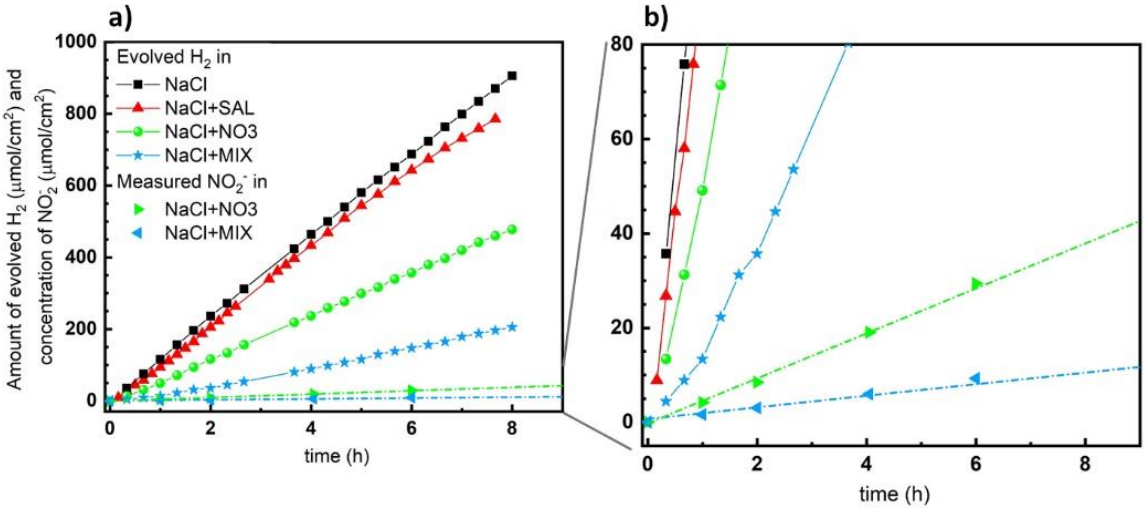

Figure 4. a) Hydrogen evolution and formation of nitrites (NO_2^-) during discharge in 3.5% NaCl with additives at current density 5 mA/cm^2. b) Magnified area of the results from a).

The experimental details are given in Supporting Materials. Micrographs of the samples after discharge in NaCl and in MIX (NO_3^-+SAL) solutions and schematic representation of the experimental set up are shown in Figure 4a and b, respectively**.** The gradient of pH and dissolved oxygen (DO) were recorded starting in the bulk electrolyte and moving towards the corroding surface. The profile lines are visualizing the DO and pH gradient in the electrolyte. The results showed high consumption of oxygen over the anode which was further influenced by the kind of additive used. Remarkably, the concentration of dissolved oxygen was considerably higher for electrolyte with NO_3^- compared to those measured for NaCl, SAL or MIX (Figure 5 (c)*)*. It has been found that both nitrate and oxygen compete for the cathodic reaction with magnesium to withdraw its electrons. However the ratio between two cathodic possesses (eq. 1 and 3) is hard to establish. Since the oxygen reduction on the Mg surface is faster than the rate of diffusion of oxygen from the bulk electrolyte to the metal surface (DO_2= 2.4e-9 m^{2}s^{-1} [30]), we assume at

discharge conditions the contribution of oxygen reduction to the cathodic process would play a minor role.

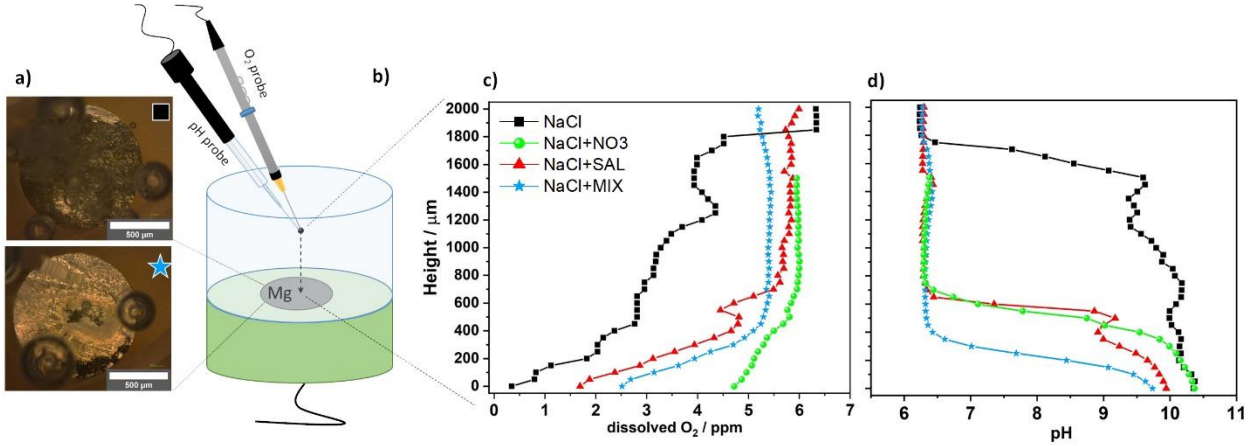

Figure 5 a) Optical micrographs of CP-Mg surface after 3h in 3.5% NaCl and in 3.5% NaCl with MIX discharge at 1mA/cm^2, b) the schematics of localized measurements of profile line for c) dissolved O_2 and d) pH over the surface.

A limited number of studies used spatially resolved techniques to visualize the local pH changes during Mg corrosion [33-40], and even less is known about **pH over the surface** when Mg is polarized [35]. Meanwhile, the local conditions are critical for the formation of $Mg(OH)_2$ precipitates [41]. In this work, the local pH gradient was measured from 2000 µm to 50 µm above the surface during Mg discharge (Figure 5 (d)). The pH increase over the surface was observed for all the samples. In the point closest to the Mg surface, i.e. 50 µm above it, the local pH was equal to 10.4 in the NaCl electrolyte and that with NO_3^-. pH stayed below 10.5 due to the formation of the corrosion products $Mg(OH)_2$ (solubility constant Ksp=5.61E-12 [42]). For SAL it was 9.9 and for MIX 9.7. The lower pH is attributed to the ability of SAL to form soluble complexes with Fe^{3+} and Mg^{2+}. In order to

connect the electrolyte pH, formation of precipitates $Mg(OH)_2$ and formation of Mg complexes, thermodynamic factors of the system were explored by plotting equilibrium diagrams (Figure 6).

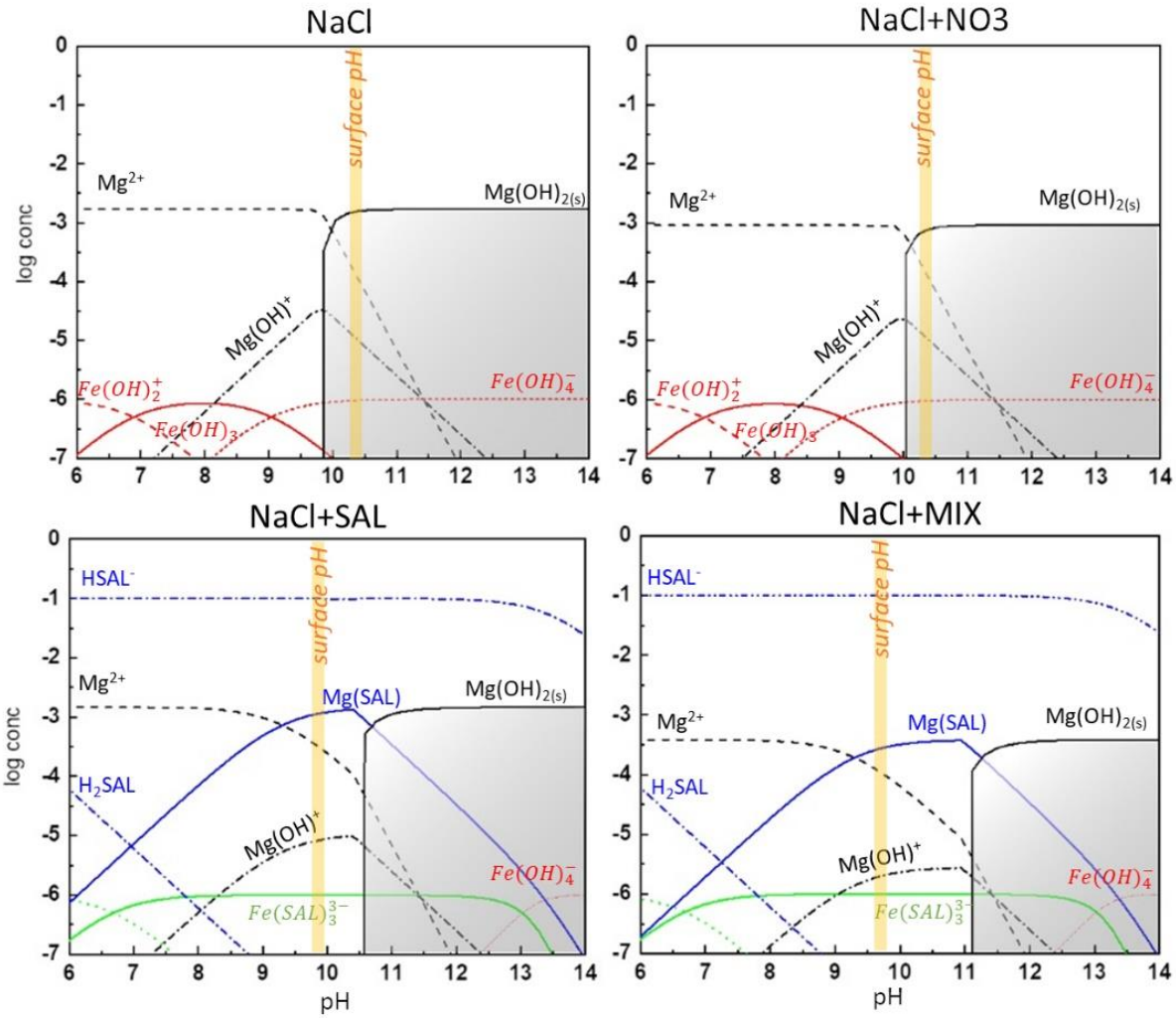

Figure 6 Thermodynamic equilibrium of the electrolyte with different additives after 3h discharge at 5mA/cm^2. Calculation made by Hydra/Medusa software[43]. Yellow line corresponds to measured pH on the surface and gray areas indicate the pH at which $Mg(OH)_2$ precipitates.

According to Figure 6, the critical pH of $Mg(OH)_{2(s)}$ formation is lower than the measured pH over Mg (identified as vertical line); therefore solid corrosion products are formed on the surface for NaCl and in NaCl+NO3 electrolytes. For both electrolytes with SAL the pH over the surface was

lower than 10, and the pH of formation of precipitates is shifted to more alkaline region due to formation of soluble Mg- SAL complexes. The lower pH and also lower hydrogen evolution indicates that MIX greatly reduced the corrosion of Mg. Possibly, it is due to the ability of SAL to complex dissolved Fe^{3+} ($logK^{st}_{Fe^{3+}}$= 35.31 [44]) and hinder further iron redeposition [21]. Formation of strong complexes between Fe and SAL is possible in pH range between 5.5 and 13.5, which makes them effective inhibitor for Fe redeposition in a wide pH range. Additionally, the ability of SAL to form soluble complexes with Mg ($logK^{st}_{Mg^{2+}} = 5.2$ [44]) helps to prevents the formation of corrosion products on the anode surface [14]. Notably, when SAL and nitrate anions are mixed, clear improvement in utilization efficiency was observed up to 82%, with no losses in the cell voltage. Moreover, no corrosion products were found in the micrographs under SEM imaging (Figure 2g,h). We hypothesis that such behavior is related to the synergistic effect of NO3- and SAL towards inhibition of intensive self-corrosion under polarization. The possible origin of such behavior could be related to the Fe replating mechanism. The confirmation of the latter statement was obtained using a high purity magnesium (HP-Mg) as an anode with low amount of Fe impurities (iron content was 51 ppm, Table S1). The comparison of the discharge curves and respective utilization efficiencies are shown in Figure 7. The low self-corrosion rate of HP-Mg leads to higher utilization efficiency and lower potential as compared to the CP-Mg. However, the utilization efficiency and operating voltage of HP-Mg were impaired in the presence of additives in the electrolyte. Note that Mg used for practical applications is typically of lower purity because it is cheaper and easier accessible.

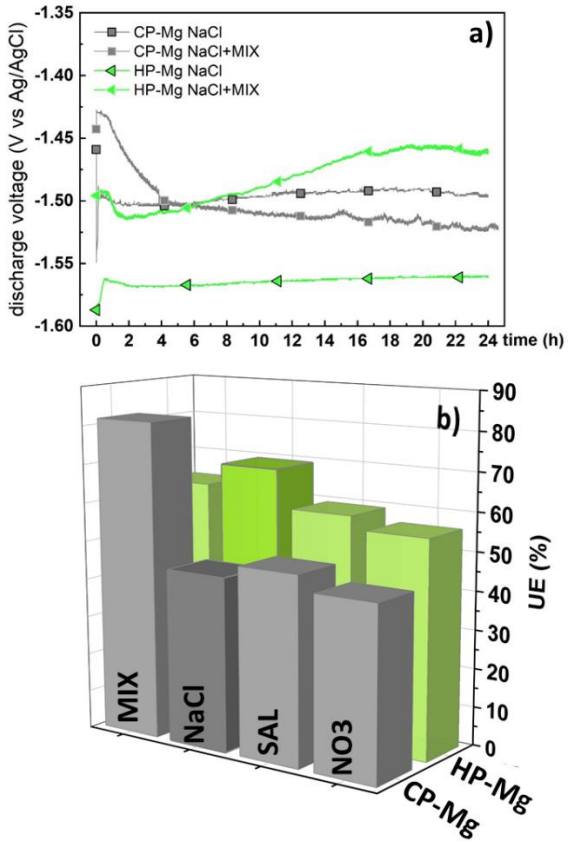

Figure 7 Comparison of (a) the discharge curves and (b) utilization efficiency of the different purity Mg anode. HP-Mg corresponds to high purity magnesium. CP-Mg corresponds to commercially pure Mg.

Thus, the discovered synergistic mixture of additives is of applied interest. Considering the results above the expected mechanism for the mixture of SAL and nitrates is shown in Figure 8. The strongest complexation and thus, the highest inhibiting effect, from SAL is expected with tri-valent iron. Nitrate ions present in the electrolyte facilitate iron dissolution with further oxidation to Fe^{3+}. This hypothesis is supported by the fact that iron is used as an effective metal for removal of the nitrate impurities in wastewater due to the high propensity of iron for NO_3^- reduction [45-46]. The dissolved Fe^{3+} promotes the complex formation with SAL. As a consequence, the iron re-deposition is hindered and, thus, the decrease of the cathodically active spots.

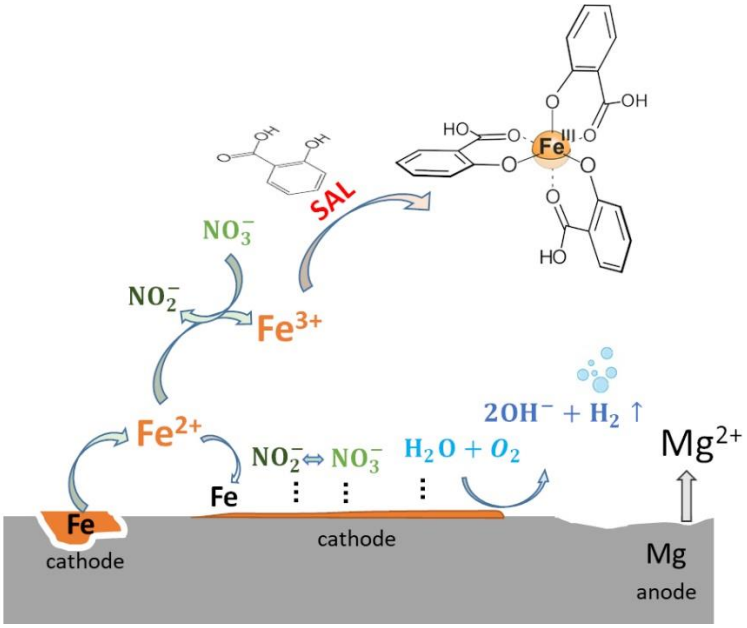

Figure 8. Proposed mechanism of synergistic inhibition of self-corrosion by mixture of NO_3^- and SAL during discharge of CP-Mg anode.

In conclusion, the obtained results demonstrate that the combination of electrolyte additives greatly improves the discharging behavior of the primary Mg battery by (i) minimizing self-corrosion, suppressing the hydrogen evolution reaction, and (ii) achieving uniform dissolution of the Mg anode with subsequent suppression of chunk effect. The proposed electrolyte able to maintain the surface of the anode free of corrosion products and minimize the formation of corrosion products on air cathode, improving electrodes capacity. A great leap is already accomplished with the synergistic approach to use a mixture of electrolyte additives. The approach to use a mixture of electrolyte additives is intriguing and elevate the performance of the Mg-air batteries to a higher level. Thus, there is a need for more research on the mixture of additive for the electrolyte of primary Mg-air batteries.

ASSOCIATED CONTENT

Supporting Information

The Experimental procedures, materials, localized measurements and information about quantification of nitrites.

AUTHOR INFORMATION

Corresponding author

e-mail: darya.snihirova@hzg.de

The authors declare no competing financial interests.

ACKNOWLEDGMENT

The authors appreciate the help of Dr. J.Bohlen and his team for the help with extrusion experiment, D.Strerath for nitrite quantification and U.Burmester with sample preparation for localized measurements and V. Heitmann for technical support. The financial support was done via SeaMag project (MarTERA ERA-NET cofund). L. Wang, C. Wang and M. Deng are grateful for the award of fellowship from China Scholarship Council (No. 201706370183, No. 201806310128 and No. 201606370031).

REFERENCES

1. Li, C.-S.; Sun, Y.; Gebert, F.; Chou, S.-L., Current Progress on Rechargeable Magnesium–Air Battery. *Advanced Energy Materials* **2017**, 1700869-n/a.
2. Li, Y.; Lu, J., Metal–Air Batteries: Will They Be the Future Electrochemical Energy Storage Device of Choice? *ACS Energy Letters* **2017,** *2* (6), 1370-1377.
3. Deng, M.; Höche, D.; Snihirova, D.; Wang, L.; Vaghefinazari, B.; Lamaka, S. V.; Zheludkevich, M. L., CHAPTER 12 Aqueous Mg Batteries. In *Magnesium Batteries: Research and Applications*, The Royal Society of Chemistry: 2020; pp 275-308.
4. Sun, Y.; Liu, X.; Jiang, Y.; Li, J.; Ding, J.; Hu, W.; Zhong, C., Recent advances and challenges in divalent and multivalent metal electrodes for metal–air batteries. *Journal of Materials Chemistry A* **2019,** *7* (31), 18183-18208.

5. Yuan, S.; Lu, H.; Sun, Z.; Fan, L.; Zhu, X.; Zhang, W., Electrochemical Performance of Mg-3Al Modified with Ga, In and Sn as Anodes for Mg-Air Battery. *J Electrochem Soc* **2016,** *163* (7), A1181-A1187.
6. Deng, M.; Höche, D.; Lamaka, S. V.; Snihirova, D.; Zheludkevich, M. L., Mg-Ca binary alloys as anodes for primary Mg-air batteries. *J. Power Sources* **2018,** *396*, 109-118.
7. Li, X.; Lu, H.; Yuan, S.; Bai, J.; Wang, J.; Cao, Y.; Hong, Q., Performance of Mg–9Al–1In Alloy as Anodes for Mg-Air Batteries in 3.5 wt% NaCl Solutions. *J Electrochem Soc* **2017,** *164* (13), A3131-A3137.
8. Zheng, T. X.; Hu, Y. B.; Zhang, Y. X.; Yang, S. W.; Pan, F. S., Composition optimization and electrochemical properties of Mg-Al-Sn-Mn alloy anode for Mg-air batteries. *Materials & Design* **2018,** *137*, 245-255.
9. Deng, M.; Wang, L.; Höche, D.; Lamaka, S. V.; Snihirova, D.; Vaghefinazari, B.; Zheludkevich, M. L., Clarifying the decisive factors for utilization efficiency of Mg anodes for primary aqueous batteries. *J. Power Sources* **2019,** *441*, 227201.
10. Zhao, Y.; Huang, G.; Zhang, C.; Peng, C.; Pan, F., Effect of phosphate and vanadate as electrolyte additives on the performance of Mg-air batteries. *Mater. Chem. Phys.* **2018,** *218*, 256-261.
11. Richey, F. W.; McCloskey, B. D.; Luntz, A. C., Mg Anode Corrosion in Aqueous Electrolytes and Implications for Mg-Air Batteries. *J Electrochem Soc* **2016,** *163* (6), A958-A963.
12. Li, Y.; Ma, J.; Wang, G.; Ren, F.; Zhu, Y.; Song, Y., Investigation of Sodium Phosphate and Sodium Dodecylbenzenesulfonate as Electrolyte Additives for AZ91 Magnesium-Air Battery. *J Electrochem Soc* **2018,** *165* (9), A1713-A1717.
13. Zhao, Y.-C.; Huang, G.-S.; Gong, G.-l.; Han, T.-Z.; Xia, D.-B.; Pan, F.-S., Improving the Intermittent Discharge Performance of Mg–Air Battery by Using Oxyanion Corrosion Inhibitor as Electrolyte Additive. *Acta Metallurgica Sinica (English Letters)* **2016,** *29* (11), 1019-1024.
14. Höche, D.; Lamaka, S. V.; Vaghefinazari, B.; Braun, T.; Petrauskas, R. P.; Fichtner, M.; Zheludkevich, M. L., Performance boost for primary magnesium cells using iron complexing agents as electrolyte additives. *Scientific Reports* **2018,** *8* (1), 7578.
15. Höche, D.; Lamaka, S. V.; Zheludkevich, M. L. Electrolyte additives for magnesium air batteries. 16187152.0, 29.08.2017, 2016.
16. Feng, Y.; Zhang, X. L.; Wu, J. B.; Peng, C. Q.; Wang, R. C., Effects of 8-hydroxyquinoline on corrosion and discharge performance of AP65 alloy as anode for Mg-air battery. *Zhongguo Youse Jinshu Xuebao/Chinese Journal of Nonferrous Metals* **2019,** *29* (12), 2738-2746.
17. Hoche, D.; Blawert, C.; Lamaka, S. V.; Scharnagl, N.; Mendis, C.; Zheludkevich, M. L., The effect of iron re-deposition on the corrosion of impurity-containing magnesium. *Physical Chemistry Chemical Physics* **2016,** *18* (2), 1279-1291.
18. Mercier, D.; Światowska, J.; Zanna, S.; Seyeux, A.; Marcus, P., Role of Segregated Iron at Grain Boundaries on Mg Corrosion. *J Electrochem Soc* **2018,** *165* (2), C42-C49.
19. Liu, X.; Xue, J.; Zhang, P.; Wang, Z., Effects of the combinative Ca, Sm and La additions on the electrochemical behaviors and discharge performance of the as-extruded AZ91 anodes for Mg-air batteries. *J. Power Sources* **2019,** *414*, 174-182.
20. Lamaka, S. V.; Hoche, D.; Petrauskas, R. P.; Blawert, C.; Zheludkevich, M. L., A new concept for corrosion inhibition of magnesium: Suppression of iron re-deposition. *Electrochem Commun* **2016,** *62*, 5-8.

21. Lamaka, S. V.; Vaghefinazari, B.; Mei, D.; Petrauskas, R. P.; Höche, D.; Zheludkevich, M. L., Comprehensive screening of Mg corrosion inhibitors. *Corros Sci* **2017,** *128*, 224-240.
22. Vaghefinazari, B.; Höche, D.; Lamaka, S. V.; Snihirova, D.; Zheludkevich, M. L., Tailoring the Mg-air primary battery performance using strong complexing agents as electrolyte additives. *J. Power Sources* **2020,** *453*, 227880.
23. Wang, L.; Snihirova, D.; Deng, M.; Vaghefinazari, B.; Lamaka, S. V.; Höche, D.; Zheludkevich, M. L., Tailoring electrolyte additives for controlled Mg-Ca anode activity in aqueous Mg-air batteries. *J. Power Sources* **2020,** *460*, 228106.
24. Ma, J.; Wang, G.; Li, Y.; Li, W.; Ren, F., Influence of Sodium Silicate/Sodium Alginate Additives on Discharge Performance of Mg–Air Battery Based on AZ61 Alloy. *J. Mater. Eng. Perform.* **2018,** *27* (5), 2247-2254.
25. Maltseva, A.; Lamaka, S. V.; Yasakau, K. A.; Mei, D.; Kurchavov, D.; Zheludkevich, M. L.; Lefèvre, G.; Volovitch, P., In situ surface film evolution during Mg aqueous corrosion in presence of selected carboxylates. *Corros Sci* **2020**, 108484.
26. Wang, S. Y.; Li, Q.; Zhong, X. K.; Li, L. Q.; Chen, F. N.; Luo, F.; Dai, Y.; Gao, H.; Liu, F.; Zhang, H. X., Effects of NO 3 - in NaCl solution on corrosion protection of AZ91D magnesium alloy coated with silane films. *Transactions of the Institute of Metal Finishing* **2012,** *90* (2), 78-85.
27. Snihirova, D.; Taryba, M.; Lamaka, S. V.; Montemor, M. F., Corrosion inhibition synergies on a model Al-Cu-Mg sample studied by localized scanning electrochemical techniques. *Corros Sci* **2016,** *112*, 408-417.
28. Silva, E. L.; Lamaka, S. V.; Mei, D.; Zheludkevich, M. L., The Reduction of Dissolved Oxygen During Magnesium Corrosion. *ChemistryOpen* **2018,** *7* (8), 664-668.
29. Taryba, M. G.; Montemor, M. F.; Lamaka, S. V., Quasi-simultaneous mapping of local current density, pH and dissolved O2. *Electroanalysis* **2015,** *27*, 1-7.
30. Snihirova, D.; Hoche, D.; Lamaka, S.; Mir, Z.; Hack, T.; Zheludkevich, M. L., Galvanic corrosion of Ti6Al4V-AA2024 joints in aircraft environment: Modelling and experimental validation. *Corros Sci* **2019,** *157*, 70-78.
31. Lamaka, S. V.; Taryba, M.; Montemor, M. F.; Isaacs, H. S.; Ferreira, M. G. S., Quasi-simultaneous measurements of ionic currents by vibrating probe and pH distribution by ion-selective microelectrode. *Electrochem Commun* **2011,** *13* (1), 20-23.
32. Wang, C.; Mei, D.; Wiese, G.; Wang, L.; Deng, M.; Lamaka, S.; Zheludkevich, M., High Rate Oxygen Reduction Reaction during Corrosion of Ultra-High-Purity Magnesium. *submited* **2020**.
33. Lamaka, S. V.; Knörnschild, G.; Snihirova, D. V.; Taryba, M. G.; Zheludkevich, M. L.; Ferreira, M. G. S., Complex anticorrosion coating for ZK30 magnesium alloy. *Electrochim Acta* **2009,** *55* (1), 131-141.
34. Izquierdo, J.; Nagy, L.; Bitter, I.; Souto, R. M.; Nagy, G., Potentiometric scanning electrochemical microscopy for the local characterization of the electrochemical behaviour of magnesium-based materials. *Electrochim Acta* **2013,** *87*, 283-293.
35. Izquierdo, J.; Fernández-Pérez, B. M.; Filotás, D.; Őri, Z.; Kiss, A.; Martín-Gómez, R. T.; Nagy, L.; Nagy, G.; Souto, R. M., Imaging of Concentration Distributions and Hydrogen Evolution on Corroding Magnesium Exposed to Aqueous Environments Using Scanning Electrochemical Microscopy. *Electroanalysis* **2016,** *28* (10), 2354-2366.

36. Lamaka, S. V.; Gonzalez, J.; Mei, D.; Feyerabend, F.; Willumeit-Römer, R.; Zheludkevich, M. L., Local pH and Its Evolution Near Mg Alloy Surfaces Exposed to Simulated Body Fluids. *Advanced Materials Interfaces* **2018,** *5* (18).
37. Dauphin-Ducharme, P.; Asmussen, R. M.; Tefashe, U. M.; Danaie, M.; Binns, W. J.; Jakupi, P.; Botton, G. A.; Shoesmith, D. W.; Mauzeroll, J., Local hydrogen fluxes correlated to microstructural features of a corroding sand cast AM50 magnesium alloy. *J Electrochem Soc* **2014,** *161* (12), C557-C564.
38. Jamali, S. S.; Moulton, S. E.; Tallman, D. E.; Forsyth, M.; Weber, J.; Wallace, G. G., Applications of scanning electrochemical microscopy (SECM) for local characterization of AZ31 surface during corrosion in a buffered media. *Corros Sci* **2014,** *86*, 93-100.
39. Dauphin-Ducharme, P.; Asmussen, R. M.; Shoesmith, D. W.; Mauzeroll, J., In-situ Mg2+ release monitored during magnesium alloy corrosion. *Journal of Electroanalytical Chemistry* **2015,** *736*, 61-68.
40. Tefashe, U. M.; Dauphin-Ducharme, P.; Danaie, M.; Cano, Z. P.; Kish, J. R.; Botton, G. A.; Mauzeroll, J., Localized corrosion behavior of AZ31B magnesium alloy with an electrodeposited poly (3,4-Ethylenedioxythiophene) Coating. *J Electrochem Soc* **2015,** *162* (10), C536-C5744.
41. Maltseva, A.; Shkirskiy, V.; Lefèvre, G.; Volovitch, P., Effect of pH on Mg(OH)2 film evolution on corroding Mg by in situ kinetic Raman mapping (KRM). *Corros Sci* **2019,** *153*, 272-282.
42. Dean, J. A., *Lange's Handbook of Chemistry*. McGraw-Hill Inc.: USA, 1999.
43. Puigdomenech, I., Program MEDUSA (Make equilibrium diagrams using sophisticated algorithms). Technology, R. I. o., Ed. Stockholm, 1999.
44. Martell, A.; Smith, R., *Critical stability contants. First Supplement.* New York, 1982; Vol. 5.
45. Ezzatahmadi, N.; Ayoko, G. A.; Millar, G. J.; Speight, R.; Yan, C.; Li, J.; Li, S.; Zhu, J.; Xi, Y., Clay-supported nanoscale zero-valent iron composite materials for the remediation of contaminated aqueous solutions: A review. *Chem. Eng. J.* **2017,** *312*, 336-350.
46. Liu, Y.; Wang, J., Reduction of nitrate by zero valent iron (ZVI)-based materials: A review. *Sci. Total Environ.* **2019,** *671*, 388-403.